Multiscale Design of 3D GDE Breaks Mass Transport Barriers for Efficient H_2O_2 Electrosynthesis

Shijie Zhang[a], Zhenyang Dong[a], Wenjuan Fang[a], Zhikang Bao[b], Zaixiang Xu[a], Yunyi Cao[d], Nan Lin[*c], Haibo Lin[c], Yuheng Wang[*d] and Jianguo Wang[*a]

[a] Institute of Industrial Catalysis, State Key Laboratory of Green Chemical Synthesis and Conversion, College of Chemical Engineering, Zhejiang University of Technology, Hangzhou 310014, P.R. China.

[b] College of Chemical and Material Engineering, Quzhou University, Quzhou 324000, China.

[c] State Key Laboratory of Inorganic Synthesis & Preparative Chemistry, College of Chemistry, Jilin University, Changchun, 130012, China.

[d] Advanced Technology Center, Wuxi Little Swan Electric Co., Ltd, Wuxi 214125, Jiangsu, China.

[*]Corresponding author. E-mail: nanlin@jlu.edu.cn, wangyh227@midea.com, and jgw@zjut.edu.cn

1. Experimental section

1.1 Chemicals and materials

Gas diffusion layer (GDL, YLS30T) and anion exchange membrane (FAB-PK-130) was purchased from Suzhou Sinero Technology CO., Ltd. MMO (IrO_2-Ta_2O_5/Ti 4×7 cm^2) and MMO (Pt/Ti 4×7 cm^2) were obtained from Shuertai CO., (Suzhou). Anion exchange membrane (FAA-3-PK-130) was obtained from Suzhou Sinero Technology Co., Ltd. Sodium sulfate (Na_2SO_4, 99%) and potassium titanyl oxalate ($C_4H_2K_2O_{10}Ti$, 98%) was purchased from Aladdin Industrial Corporation. Nafion solution was obtained from Shanghai Branch, Du Pont China Holding Co., Ltd. Ethyl alcohol (C_2H_5OH, ≥99.8%) was provided by Beijing Chemical Works. Deionized water (Millipore, 18.2 MΩ cm) was used as the solvent, which was made in the laboratory. All chemicals were used as received without further purification.

1.2 Catalyst characterization

The surface morphologies of the catalysts were analyzed by scanning electron microscopy (SEM; HITACHI S4700) using a high beam current and an accelerating voltage of 15 kV. Transmission electron microscopy (TEM) analysis was conducted on a Tecnai G2F30S-Twin electron microscope operated at 300 kV. Brunauer-Emmett-Teller (BET) surface area measurements and pore size distribution analyses were performed for the electrocatalysts using an ASAP2460 analyzer. For TEM imaging, sample dispersions were drop-cast onto carbon-coated copper grids and dried under ambient conditions.

1.3 Preparation of the working electrode

The preparation of the working electrode involved dispersing 4.0 mg of catalyst powder in 900 μL of ethyl alcohol combined with 100 μL of a 5 wt.% Nafion solution. The resulting mixture was subjected to sonication for approximately 30 minutes to achieve a homogeneous ink. Subsequently, 5 μL of the ink was deposited onto a polished rotating ring-disk electrode (RRDE, 0.1256 cm^2) and allowed to dry at room temperature. The catalyst loading on the electrode was determined to be 0.16 mg/cm^2.

1.4 Electrochemical test condition

All electrochemical experiments were conducted at ambient temperature utilizing

a CHI760E electrochemical workstation. The electrochemical measurements for the oxygen reduction reaction (ORR) were executed within a standard three-electrode configuration, comprising a rotating glassy carbon disk as the working electrode, a platinum ring electrode, a platinum wire as the counter electrode, and a saturated calomel electrode (SCE) serving as the reference electrode. The experiments were performed in an O_2-saturated 0.1 M KOH solution. All electrochemical potentials were referenced against the reversible hydrogen electrode (RHE) for calibration purposes.

Cyclic voltammetry (CV) was performed at a scan rate of 50 mV/s, over a potential range from 0 to 1.2 V (vs. RHE). For the ORR measurements, the scan rate was set to 10 mV/s, with a rotation speed of 1600 rpm. The selectivity for hydrogen peroxide production and the electron transfer number were quantified using established equations:

$$Selectivity_{H2O2} = 200 \times \frac{I_r}{N \times I_r \times I_d}$$

$$n = 4 \times \frac{I_d}{I_d + \frac{I_r}{N}}$$

In the equations, I_r represents the ring current (mA), while I_d denotes the absolute value of the disk current (mA). The current collection efficiency of the platinum ring electrode is defined as N = 0.42, as shown in Supporting Information Figure S3.

The faradaic efficiency (FE%) on the rotating ring-disk electrode (RRDE) was calculated using the following equations:

$$FE\% = 100 \times \frac{I_r}{N \times I_d}$$

Electrochemical impedance spectroscopy (EIS) was employed to evaluate the conductivity of the catalysts at the open-circuit potential, spanning a frequency range from 0.01 to 1×10^5 Hz.

1.5 Electrochemical measurements of the surface catalyst on the 3D GDE

Electrochemical performance of the surface catalyst on the 3D GDE was initially evaluated using a rotating ring-disk electrode (RRDE). Linear sweep voltammetry (LSV) measurements revealed an onset potential for the active carbon catalyst, with H_2O_2 selectivity reaching 81.72% at 0.4 V (vs. RHE) (Figure S4). The electron transfer

number, derived from LSV data, indicated a $2e^-$ ORR pathway. The electrochemical surface area (ECSA) was 0.116 mF/cm² (Figure S5), and the Tafel slope (Figure S6) confirmed good catalytic performance. These tests laid the foundation for electrolysis experiments in the home-made reactor with 3D GDE (Figure S7).

1.6 Chemical Quantification of H_2O_2 Product

The spectrophotometer (Shanghai Spectrum SP-752PC) was carried out to quantified the yield of the H_2O_2 through the potassium-titanium oxalate method, in which the formation of titanium (IV)-peroxide complex in the presence of sulfuric acid. Specially, 1 mL sample was added into the as-prepared solution with 2 mL potassium titanium oxalate $C_4H_2K_2O_{10}Ti$ and 2 mL 3 M H_2SO_4. The color of the solution changes into yellow and UV-vis technology was used to calculate the content of the H_2O_2 in the samples at 400 nm (The corresponding standard curve is in Figure S8). The linear relationship between the concentration of H_2O_2 and the absorbance was: $A=0.02011+0.01035\times C$ ($R^2=0.9989$).

2. Modelling information

2.1 Computational information

The 2D multiphysics model consists of nine partial differential equations (PDEs) and associated constitutive relations, implemented and solved using COMSOL Multiphysics 6.2. The meshing uses a self-adaptive free quadrilateral grid with 2047 domain elements and 276 boundary elements. All simulations were run on a supercomputer equipped with a 96-core Intel(R) Xeon(R) Platinum 9242 processor.

2.2 Boundary conditions

For CFD part, the fluids at all walls except blowholes of anode chamber ($y = 0$) and liquid levels ($y = H_1 + H_3$) are considered as no slip velocity $u_l \cdot n = 0$ and no gas flux $N_g \cdot n = 0$. In the cathode chamber, at the blowholes on the bottom ($y = 0$), the gas flux is set

$$-N_g \cdot n|_{x = holes,\ y = 0} = N_{O_2} = \frac{\rho_{O_2} V_{O_2}}{hA_{hole}} \left(\frac{V_{O_2}}{V_{O_2,0}} \right)^{1.9}. \quad [S1]$$

In the anode chamber, on the electrode at the bottom, the gas flux meets the condition,

$$-N_g \cdot n|_{y=0} = \frac{i_a}{nM_{O_2}F}, \quad [S2]$$

where M_{O_2} is the molar mass of oxygen. At the liquid level of all chambers, it is considered that there is no liquid slip $u_l \cdot n = 0$ and gas outlets $\rho_g s_g = 0$.

The liquid pressure constraints are set at the points,

$$p|_{(x=0,\ y=H_3)} = p|_{(x=2L+d_{m'},\ y=H_3)} = 0. \quad [S3]$$

For electrochemical part, on the cathode, the applied current is set on the bottom,

$$\int_{\partial y=0} i \cdot n dx = -I_{app}, \quad [S4]$$

and on the anode, it follows

$$\int_{\partial y=0} i \cdot n dx = I_{app}. \quad [S4]$$

There is no current density at any other walls,

$$i \cdot n = 0. \quad [S5]$$

The zero potential face in the electrolyte is set at the membrane,

$$\phi|_{x=L} = 0. \quad [S6]$$

There are no species fluxes at all walls and the membrane is an AEM, in which the cations cannot transport, the discontinuity of cation transport is set at the boundary of $x = L$ and $x = L + d_m$.

2.3 Initial conditions

The initial conditions are assumed that the reactor is not proceeded. Therefore, the velocity field is

$$u_{l,0} = 0, \quad [S6]$$

pressure follows linear relationship,

$$p_0 = \rho_l g(H - y), \quad [S7]$$

and the effective gas density yields

$$\rho_g s_g|_{t=0} = 0. \quad [S8]$$

The electrolyte is considered as 0.5M Na_2SO_4, and the electrolyte potential ϕ is 0.

Table S1. The configuration data of half-cell, membrane and blowholes

Parameters	Symbols	Value
Total height (mm)	H	115
Column height (mm)	H_1	55
Connect channel height (mm)	H_2	30
Liquid level (mm)	H_3	25
AEM thickness (mm)	d_m	1
Total length (mm)	L	120
Column length (mm)	L_1	60
Connect channel length (mm)	L_2	40
Gas outlet length (mm)	L_3	30
Side channel length (mm)	L_4	33

Table S2. List of parameters and constants

Symbol	Description	Value	Unit.	Ref.
A_{hole}	Area of blowholes	2.01	mm^2	Mea.
$C_{dl,c}$	Double layer capacitance of cathode	1.16	F/m^2	Mea.
$C_{dl,a}$	Double layer capacitance of cathode	2.0×10^{-4}	F/m^2	Est.
c_{ref}	Reference concentration of OOH^-	1.0	$\mu mol/L$	Est.
$c_{ref,H}$	Reference concentration of H^+	1.0	mol/L	Est.
$c_{ref,OH}$	Reference concentration of OH^-	1.0	mol/L	Est.
D_H	Diffusion coefficient of H^+	9.3×10^{-9}	m^2/s	Est.
D_{Na}	Diffusion coefficient of Na^+	1.33×10^{-9}	m^2/s	Est.
D_{OH}	Diffusion coefficient of OH^-	5.3×10^{-9}	m^2/s	Est.
D_{OOH}	Diffusion coefficient of OOH^-	1.0×10^{-9}	m^2/s	Est.
D_{SO4}	Diffusion coefficient of SO_4^{2-}	1.06×10^{-9}	m^2/s	Est.
$d_{b,c}$	Bubble diameter in the cathode cell	6	mm	Est.
$d_{b,a}$	Bubble diameter in the anode cell	0.5	mm	Est.
$E_{00,c1}$	Nernst potential of $2e^-$ ORR	-0.065	V	[1]
$E_{00,c2}$	Nernst potential of OOH^- to H_2O	0.867	V	[1]
$E_{00,a}$	Nernst potential of $4e^-$ OER	1.23	V	[2]
F	Faraday constant	96485	C/mol	[2]
g	Gravity	9.8	m/s^2	
h	Empirical coefficient of gas flow	2000		Est.
$i_{00,c1}$	Reference exchange current density of $2e^-$ ORR	0.05	A/m^2	Est.
$i_{00,c2}$	Reference exchange current density of OOH^- to H_2O	1.2×10^{-7}	A/m^2	Est.
$i_{00,a1}$	Reference exchange current density of $4e^-$ OER	1.0×10^{-7}	A/m^2	Est.
$i_{00,a2}$	Reference exchange current density of $2e^-$ side reaction on the anode	5.0×10^{-4}	A/m^2	Est.
l_0	Initial thickness of GDL on the cathode	42	μm	Ass.
M_{O_2}	Molar mass of oxygen	32	g/mol	[2]
n_{c1}	Electron transfer number of $2e^-$ ORR	2		
n_{c2}	Electron transfer number of OOH^- to H_2O	2		
n_{a1}	Electron transfer number of $4e^-$ OER	4		
n_{a2}	Electron transfer number of $2e^-$ side reaction on the anode	2		
V	GDL molar volume	1.12×10^{-5}	m^3/mol	Ass.
α_{c1}	Transference number of $2e^-$ ORR	0.8		Est.
α_{c2}	Transference number of OOH^- to H_2O	1.51		Est.
α_{a1}	Transference number of $4e^-$ OER	2		Est.

α_{a2}	Transference number of $2e^-$ side reaction on the anode	1		Est.
μ_l	Liquid water viscosity	3.56×10^{-4}	Pa•s	[2]
ρ_l	Water density (at 353.15 K)	0.996	g/cm^3	[2]
σ	Surface tension coefficient	0.07	N/m	[3]
Abbreviations: Ass, assumption; Est, estimation; Mea, measurement.				

3. Experiment Characterization

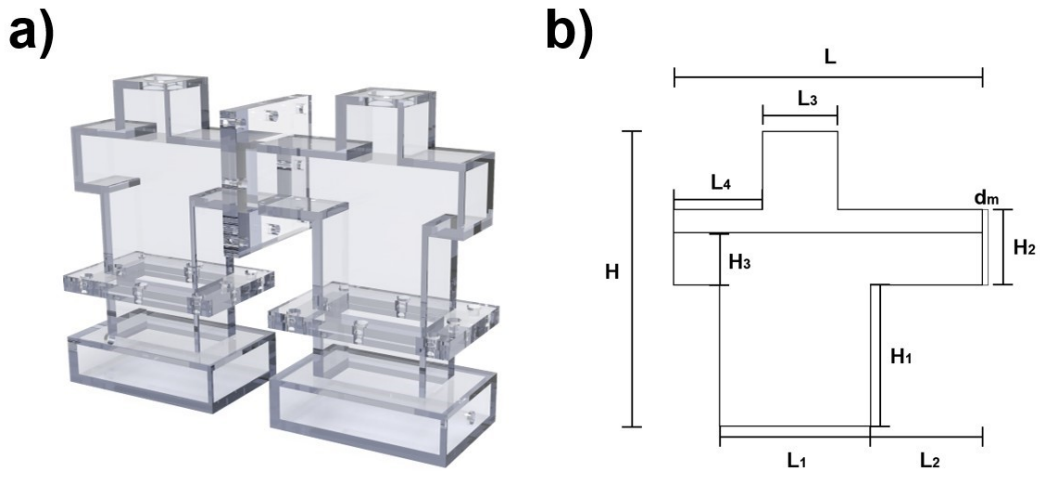

Figure S1. (a) Illustration of the real electrochemical H_2O_2 production H-cell reactor, (b) computational geometry of a half cell with the liquid level H_3.

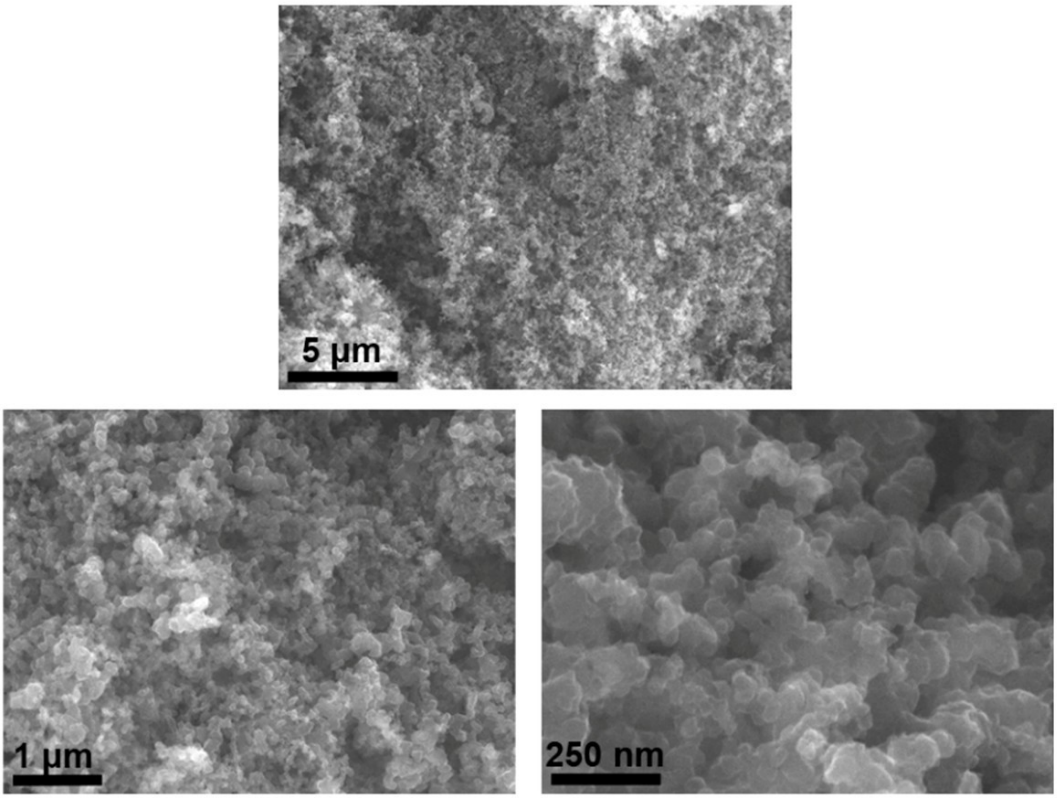

Figure S2. The SEM images of 3D GDE surface in different scales.

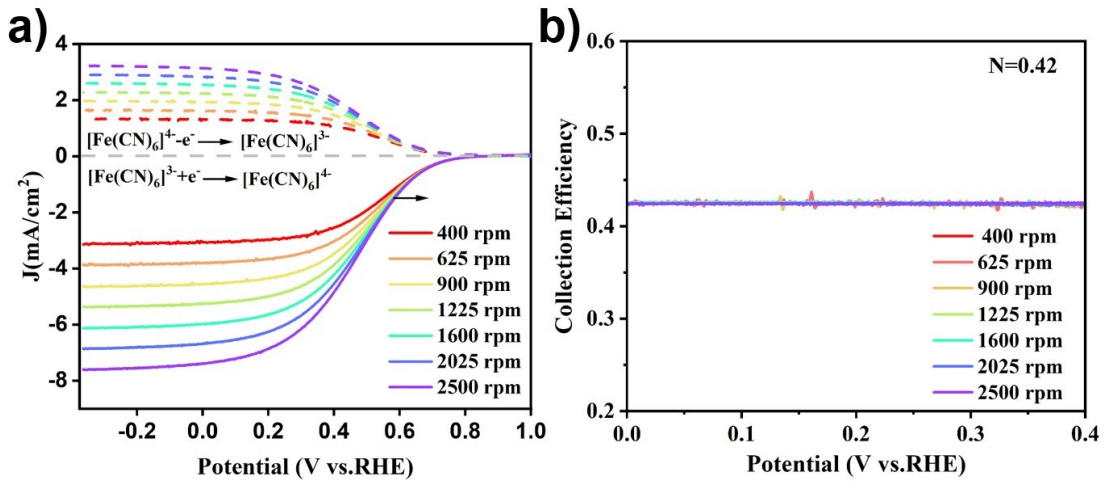

Figure S3. (a) RRDE voltammograms recorded at different rotation rates from 400 rpm to 2500 rpm. (b) The corresponding collection efficiency of RRDE voltammograms as a function of the potential.

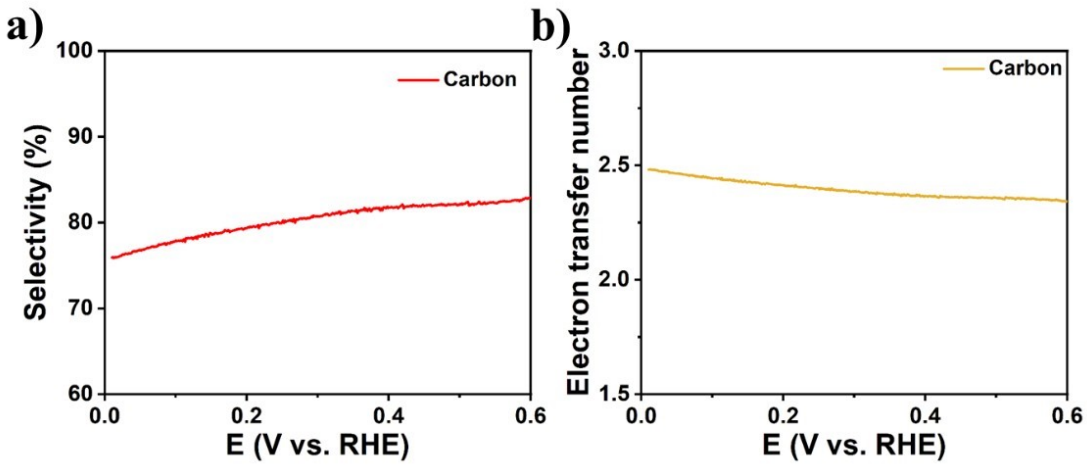

Figure S4. The H_2O_2 selectivity and electron transfer number of the catalyst.

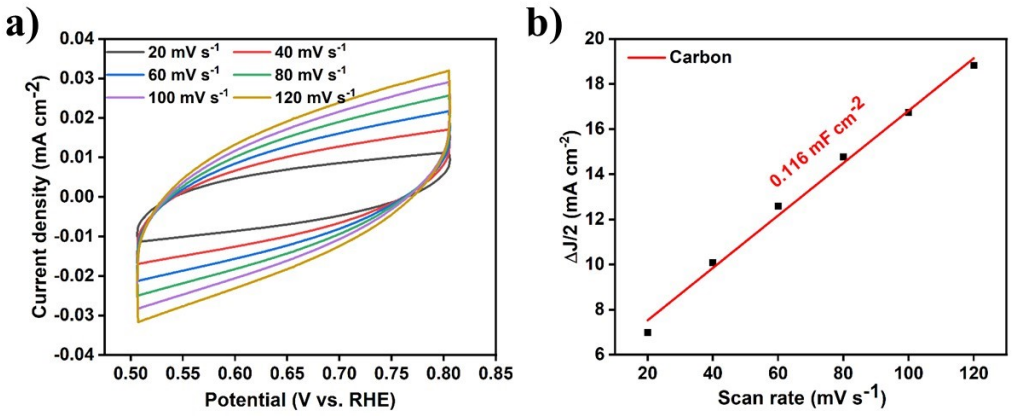

Figure S5. The H_2O_2 selectivity and electron transfer number of the catalyst.

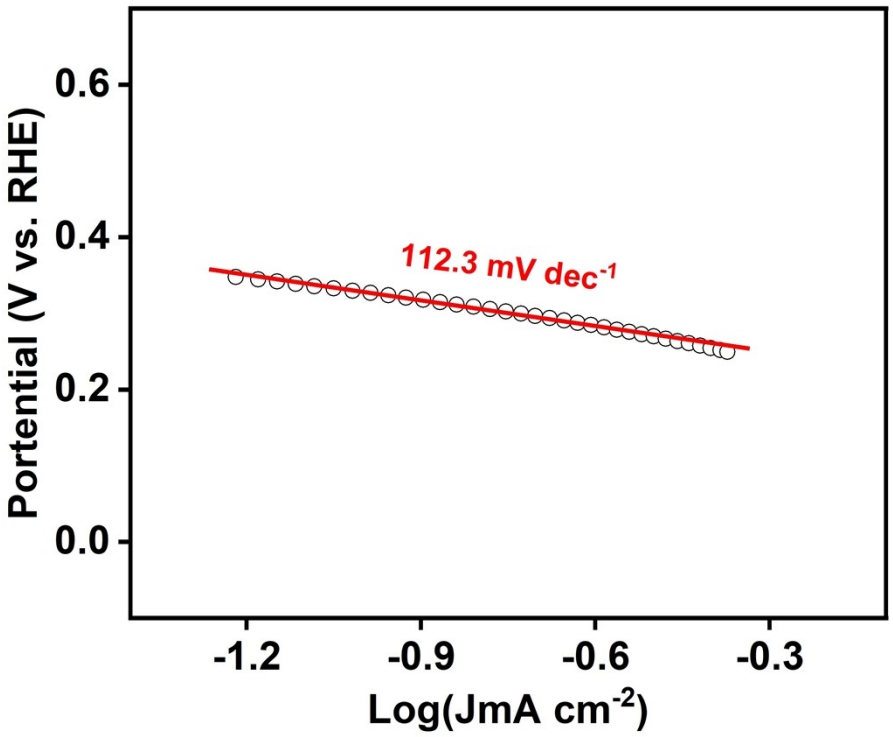

Figure S6. Tafel Slope of the catalyst.

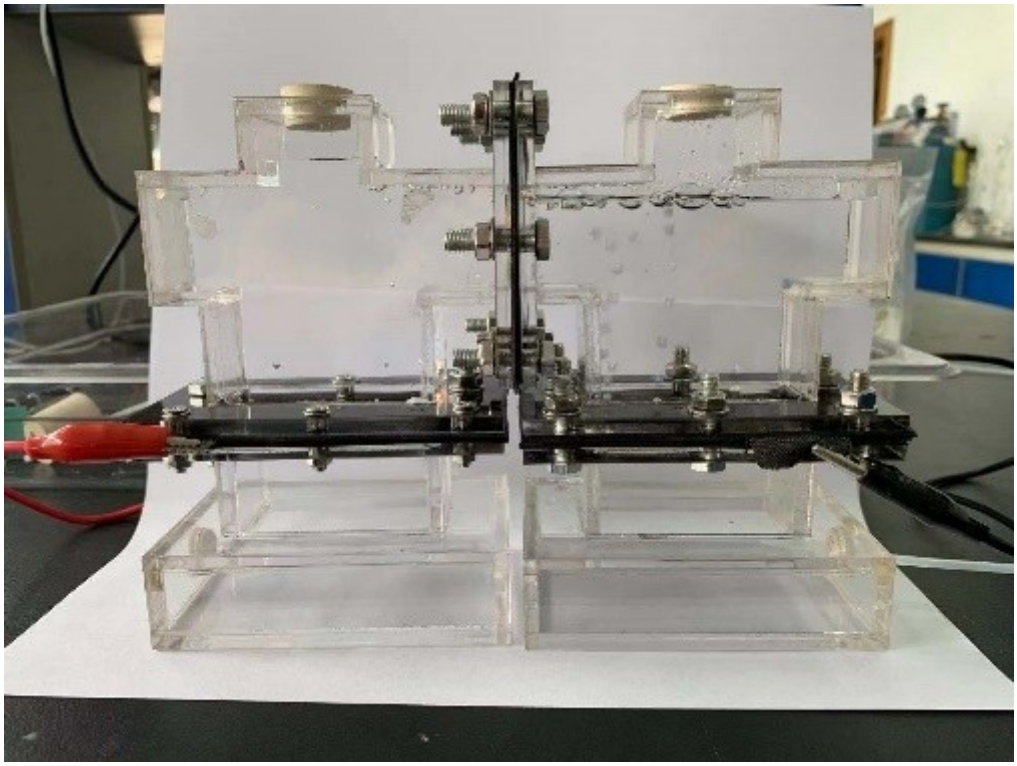

Figure S7. Image of the home-made reactor with 3D GDE.

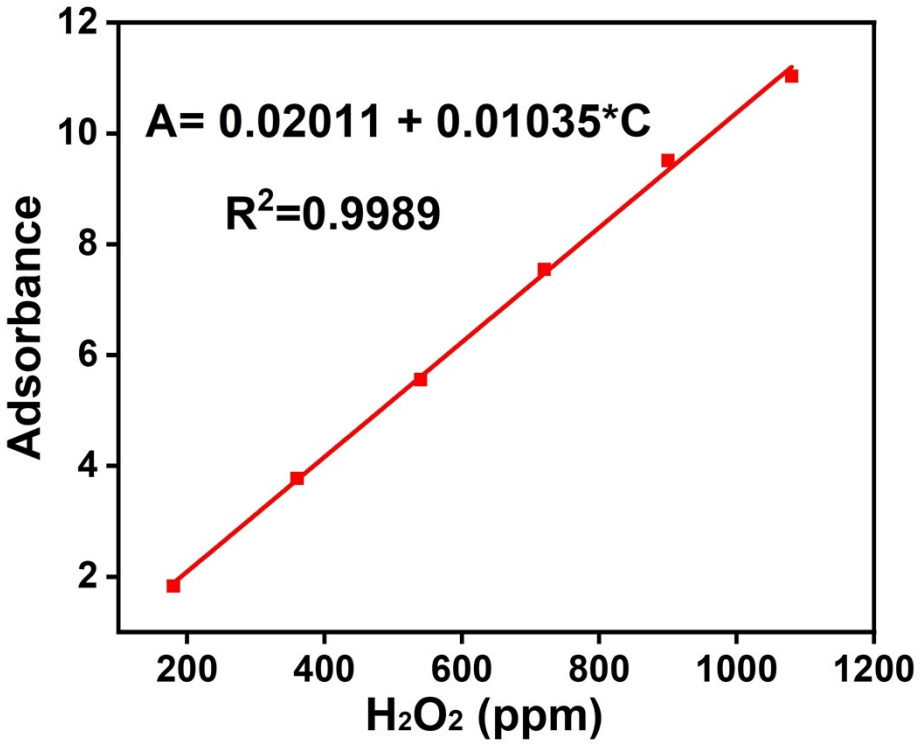

Figure S8. Absorbance spectra of standard H_2O_2 solutions (up to 4.7 mM) in mixture of 2 mL 0.05 M potassium titanium oxalate and 2 mL 3 M H_2SO_4, generating a linear calibration curve at the peak wavelength (400 nm).

Table S3. The fitting parameters of EIS equivalent circuit model for the H-cell in different working periods.

	$L/\mu H$	α	$Q/mS \cdot s^{\alpha}$	R_s/Ω	$W/mS \cdot s^{0.5}$	R_{ct}/Ω
No O_2 flow	8.41	1	18.70	47.58	3.92	∞
Initial aeration	7.54	1	22.55	50.40	3.25	∞
30 min	9.20	0.92	4.78	46.55	180.6	21.07
40 min	9.25	0.87	5.30	45.36	132.1	54.63

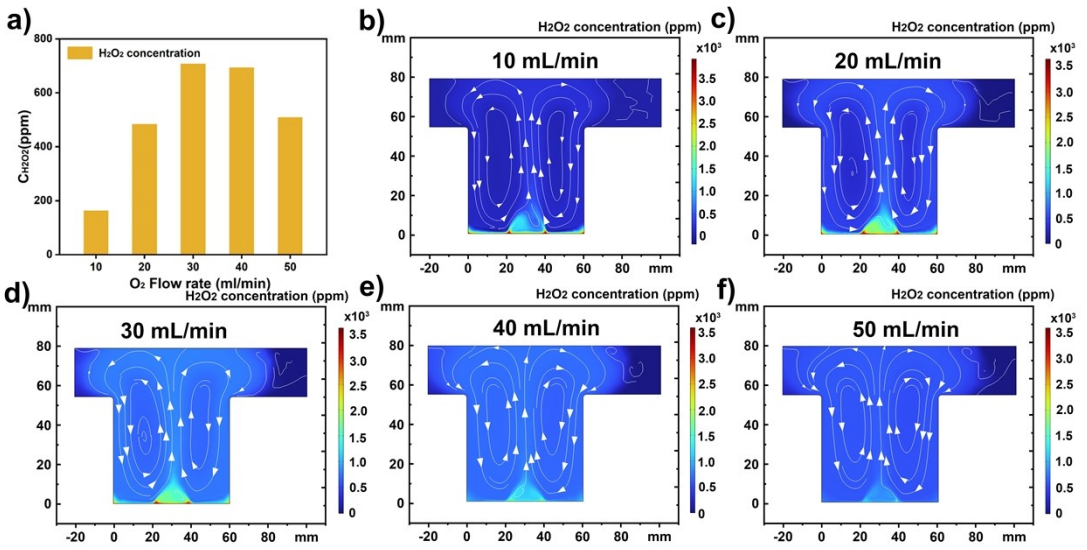

Figure S9. (a) Experimental results of H_2O_2 concentration at top sampling point at different flow rates. (b)- (f) The H_2O_2 concentration results of simulation at different O_2 flow rates (10, 20, 30, 40, and 50 mL/min) in 0.5 M Na_2SO_4 solution.

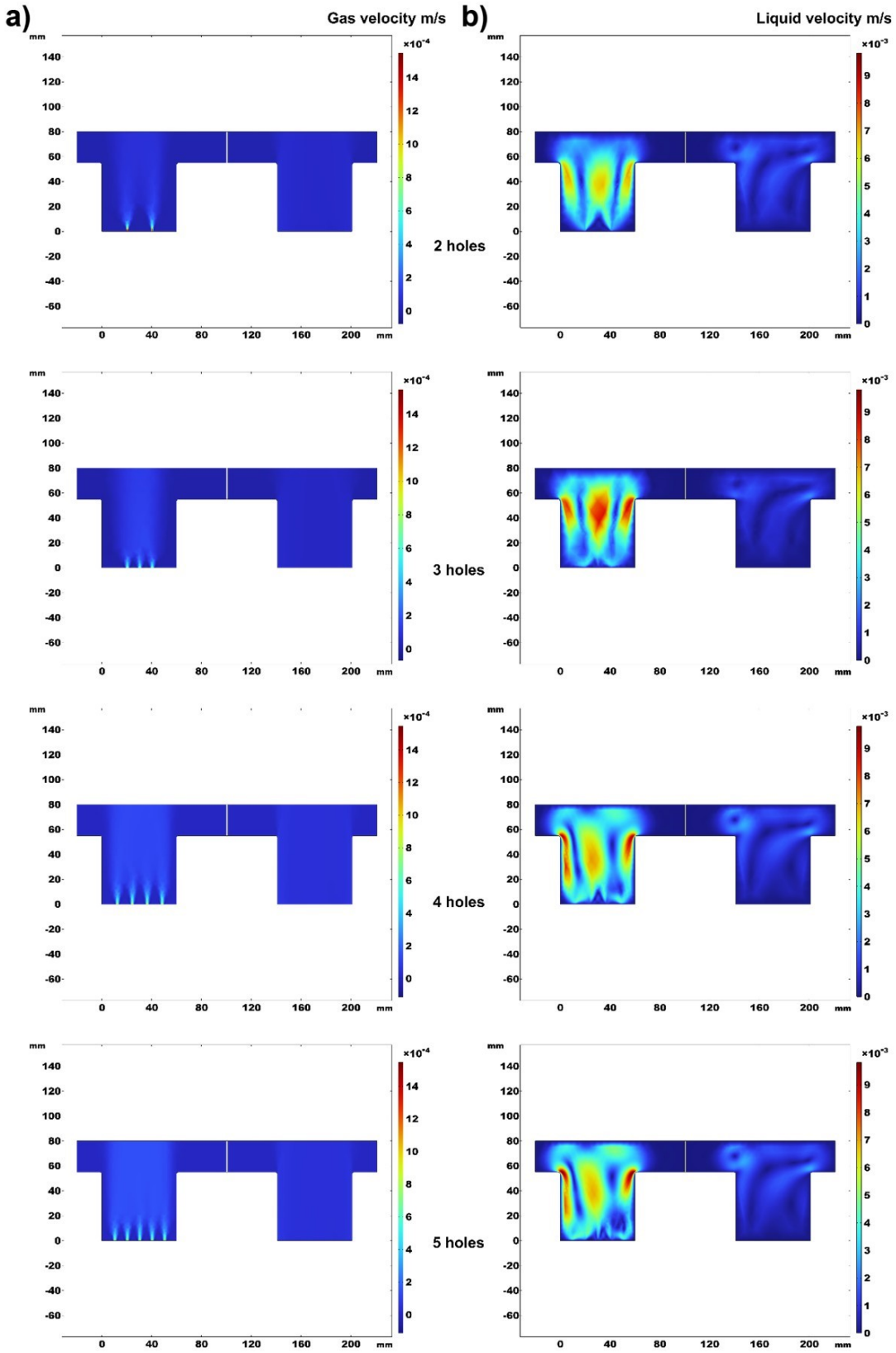

Figure S10. Velocity surface plots in the reactor for (a) gas phase and (b) liquid phase.

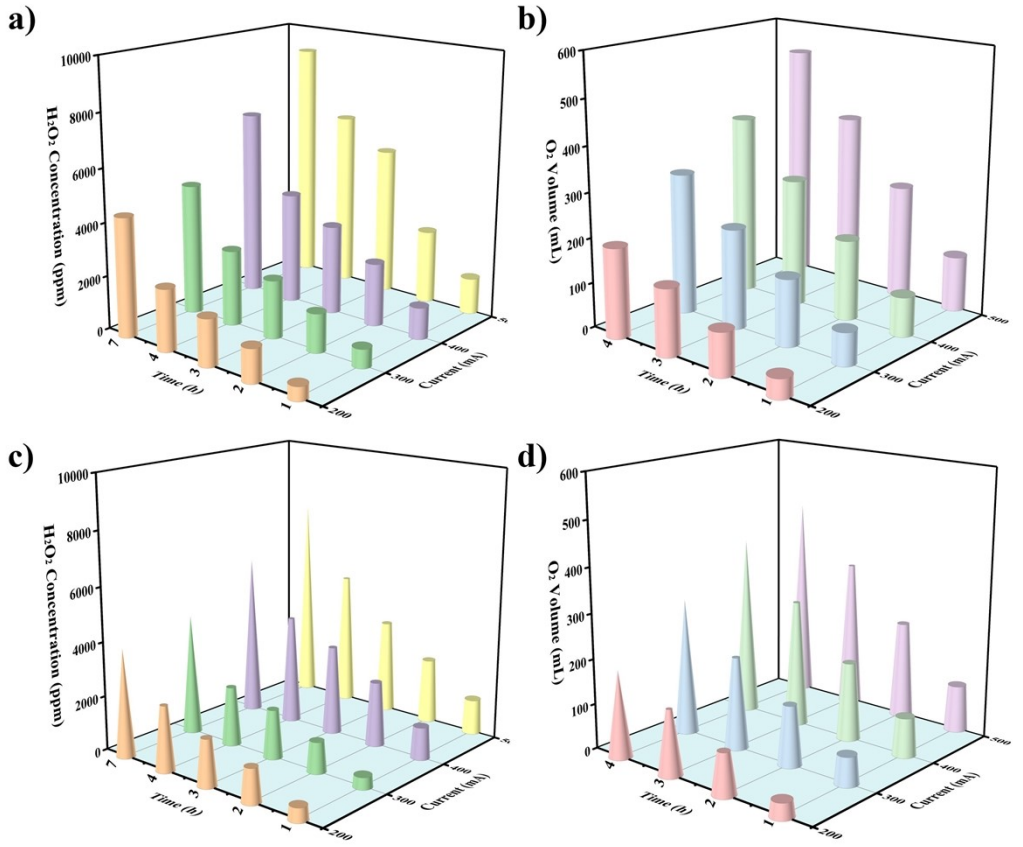

Figure S11. The yield of H_2O_2 with anode of (a) IrO_2-Ta_2O_5/Ti and (c) Pt/Ti. The yield of O_2 with anode of (b) IrO_2-Ta_2O_5/Ti and (d) Pt/Ti.

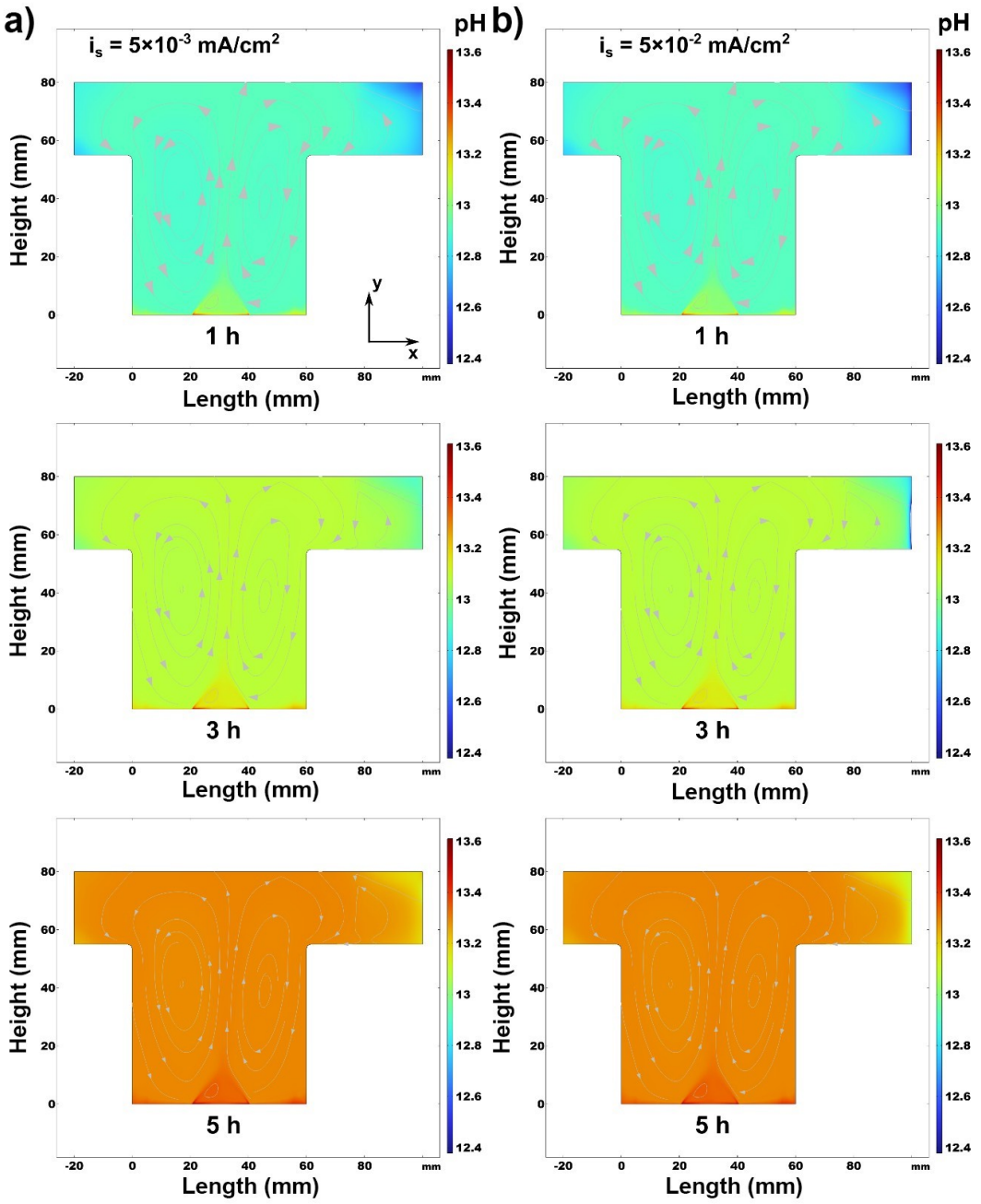

Figure S12. pH value distribution in the cathode chamber at different electrolysis time, with different anode side reaction exchange current densities (a) 5×10^{-3} mA/cm^2 and (b) 5×10^{-2} mA/cm^2.

References

1. S. Siahrostami, *Chem Catalysis*, 2023, **3**, 100568.

2. N. Lin, S. Feng and J. Wang, *AlChE J.*, 2022, **68**, e17742.

3. D. Kuzmin and S. Turek, Efficient Numerical Techniques for Flow Simulation in Bubble Column Reactors. Institute of Applied Mathematics, University of Dortmund. 2000.